Effect of Laser Microcutting on Thermo-Mechanical Properties of NiTiCu Shape Memory Alloy

Carlo Alberto Biffi[1,*], Paola Bassani[1], Marco Carnevale[2], Nora Lecis[2], Antonietta Loconte[2], Barbara Previtali[2], and Ausonio Tuissi[1]

[1]National Research Council of Italy, Institute for Energetics and Interphases, Unit of Lecco, Lecco, 23900, Italy

[2]Politecnico di Milano, Mechanical Engineering Department, Milano, 20156, Italy

1. INTRODUCTION

Shape memory alloys (SMAs) are smart and functional materials, which makes them very attractive for a variety of applications due to some well-known positive features, such as pseudo-elasticity and shape memory effect [1].

In the last few years, laser micromachining of SMAs has been considered a relevant topic from scientific and industrial points of view, mainly because these materials can be used in biomedical [2,3] and actuation and sensing applications [4-6].

Thermal effects, associated with the use of a laser beam as a source of heat during laser machining, are one of the most important and studied aspects, because they are strongly able to affect the quality of the obtained result. These effects can be amplified when temperature sensitive materials, such as SMAs, are processed using laser technology [7]. The predominant thermal modifications of these materials can be mainly associated with pulse duration and with emission wavelength in the micromachining processes [8-10].

Concerning the emission wavelength reduction, the quality of the cut edge can be significantly improved, even if the productivity of the process is greatly decreased, by lowering the power levels, as reported by Yung *et al*. [11]; moreover, the machining of metallic materials is more difficult than the machining of organics. On the contrary, the effect of the pulse duration can be appreciated in the work of Li *et al*., in which an ultrashort laser in the femtosecond regime was investigated for the microcutting of NiTi thin sheets [12]. The thermal damage was very limited and the quality of the cut edge was high, as demonstrated by the lack of melted material, which is relevant in the case of other pulse duration ranges.

In other works, the effect of process parameters that affected the quality of the cut edge were studied [13-15]. The choice of the correct shielding gas is of relevant importance in the laser micromachining of Ti alloys because of the high reactivity of Ti and its alloys. Actually, Rao *et al*. showed in a study on the CO_2 laser cutting of Ti that nitrogen and helium allow the generation of Ti nitrides while argon does not [13]. Otherwise, helium can reduce the spatter generation as well

*Corresponding author: carlo.biffi@ieni.cnr.it

as the extent of the heat affected zone (HAZ). In another work, several authors proposed an optimisation of the cut edge quality in terms of kerf geometry, spatter, HAZ extent, and roughness using Nd:YAG laser [14,15].

Another significant trend in laser technology can be associated with the diffusion of the fibre laser as an innovative laser source coming from telecommunication technology. This laser is significantly appreciated because of its obvious advantages, such as high beam quality, good focus-ability, high productivity and reliability. Some experimental studies have been proposed on laser material microprocessing, such as drilling, cutting, and milling of different materials using a fibre laser [16-20], but only a few studies have been conducted on the machining of NiTi based SMA systems, such as an NiTiCu alloy [21,22].

As reported in the literature, a relevant amount of experimental work has been proposed on the evaluation of the effect of laser material processing only for the NiTi binary system from the point of view of the processing; however, very few studies have been done of the effect of the laser machining on the peculiar characteristics of the SMAs, such as shape memory effect and pseudo-elasticity [22-25].

For these reasons, the aim of this work is to investigate the effect of microcutting using a nanosecond fibre laser on the microstructural and thermo-mechanical properties of a ternary NiTiCu SMA alloy. The NiTiCu alloy was chosen due to the lack of research available in the open literature on the laser microprocessing of this SMA system. Two process conditions, defined as two distinct microcutting speeds that would guarantee a completely open cut edge, were identified. A scanning electronic microscope (SEM) was utilised for the observation of the morphology of the laser cut edges and the chemical composition of the processed alloy was evaluated by energy dispersion spectroscopy (EDS) in different regions. Moreover, nanohardness measurements were used to estimate the heat affected zone (HAZ). To determine the functional properties of the SMA, the specific thermo-mechanical characteristics of both the base materials and the laser machined materials were studied using a Differential Scanning Calorimeter (DSC) and tensile stress/strain tests. It was shown how the fibre laser machining affects the specific SMA properties due to the effect of the thermal field imposed on the material by the laser beam. This effect can be limited by reducing the process speed parameter.

2. EXPERIMENTAL PROCEDURES

High purity Ni, Ti, and Cu metals were melted in a graphite crucible by means of a vacuum induction melting (VIM) furnace (Balzers VSG 10). The nominal composition of the produced alloy was $Ni_{40}Ti_{50}Cu_{10}$ in atomic percentage. The ingot, after hot forging and hot rolling at 950 °C, was cold straight rolled down to 150 μm thick with intermediate annealing treatments. Finally, the cold rolled sheets were heat treated at 400 °C for 1 hour, which treatment was followed by water quenching (WQ).

A pulsed nanosecond fibre laser source (YLP-50 from IPG Photonics), whose main characteristics are reported in Table 1, was used for the microcutting of the produced NiTiCu sheets. The laser system was equipped with a LaserMech cutting head for micromachining and an Aerotech motion stage. The adopted process parameters, reported in Table 2, were selected in order to guarantee a stable through-cut edge and a limited heat affected zone (HAZ). A single laser pass strategy produced an unstable cut edge, consequently a double laser pass strategy was implemented at low (5 mm/s) and high (50 mm/s) process speeds [21]. Argon flow, at a pressure of 5 bar, was utilised as an inert shielding gas for the protection of the working area and for the removal of the melted material during the laser microcutting process. The maximum available power (50 W) and the maximum pulse frequency (80 kHz) were also selected to guarantee the machining of an open kerf with a small number of laser passes. With these process conditions, the specific energy per unit of length was calculated as the ratio of the average power multiplied by the number of laser passes, divided by the process speed. With the aforementioned definition, the hypothesis that twice the power

Table 1. Main characteristics of the nanosecond fibre laser used in the experiments

Maximum average power [W]	50
Pulse frequency range [kHz]	20-80
Maximum pulse energy @50 kHz [mJ]	1.1
Minimum pulse width [ns]	100
Emission wavelength [nm]	1064
Beam quality factor	1.7
Collimated laser beam diameter [mm]	5.9

Table 2. Process parameters used in the NiTiCu laser microcutting process

Variable process parameters	
Process condition and corresponding specific energy [J/mm]	
Single pass @ 5 mm/s	10 J/mm
Double pass @ 5 mm/s	20 J/mm
Double pass @ 50 mm/s	2 J/mm
Fixed process parameters	
Pulse energy [mJ]	0.72
Pulse frequency [kHz]	80
Pulse width [ns]	160
Shielding gas	Ar
Gas pressure [bar]	5
Working distance [mm]	0.5
Focal distance [mm]	60
Laser spot diameter [μm]	23
Piercing time [ms]	0.8

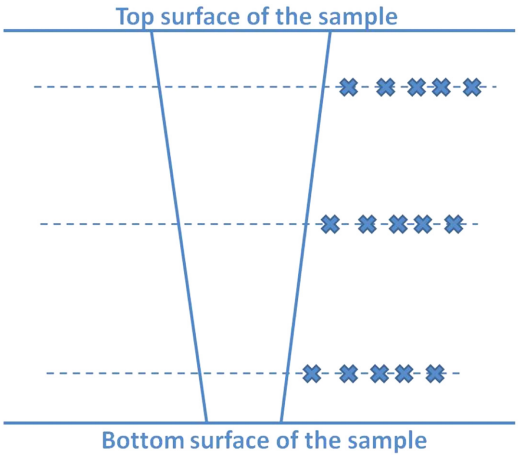

Fig. 1. Schematic representation of the regions defined for the nanohardness measurements on the transversal section.

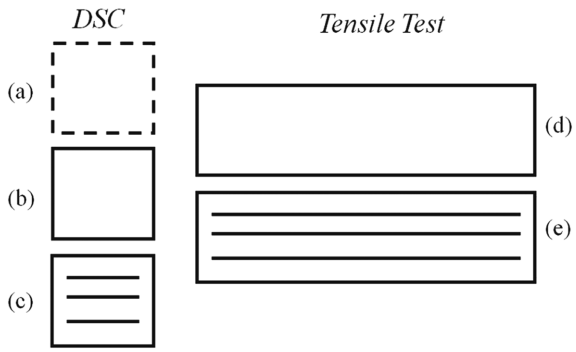

Fig. 2. Schematic representation of the different samples tested in the DSC (left) and the stress/strain characterisation (right).

was introduced into the material with the double laser pass strategy compared to the case of single pass has been taken into account.

The top and bottom surfaces of the laser cut edges, as well as several cross sections selected after conventional metallographic sample preparation, were observed by SEM. An energy dispersion spectroscopy (EDS) probe was used to analyse the compositions of both the base material and the material in proximity to the cut edge, which could include spatter or melted material, at different points.

Nanohardness measurements, measured on the transverse section of the laser cut edge, were carried out with a nanoindentator system (NHT model, CSM Instruments), equipped with a diamond Berkovich indenter and having an applied load of 10 mN. Three regions on the transversal sections were considered with respect to the proximity of the top and bottom surfaces as well as at half of the thickness of the NiTiCu sheet (see Fig. 1). The scheme, shown in Fig. 1, summarises the points in which the Vickers nanoindentations were performed. The distance between the adjacent indentations was fixed to be equidistant at approximately 10 μm.

Calorimetric analysis was performed with a DSC TA Instruments Q100, calibrated with a standard indium reference, in order to evaluate the martensitic transformation (MT) temperatures of the NiTiCu sheets. Small samples (2×2 mm^2) were prepared with the following configurations in order to evaluate the effect of the laser microcutting on the martensitic transformation behaviour (see Fig. 2):

- Mechanical Cut: this is associated with the properties of the base material and is not affected by the laser process (indicated as sample MC), as shown in Fig. 2(a);
- Periphery Laser Cut: this is a laser cut along the perimeter with a process speed of 5 mm/s (indicated as sample PLC-5), as shown in Fig. 2(b);
- Internal Laser Cut: this is a laser cut along the perimeter with three additional linear cuts inside the sample, with process speeds of 5 mm/s and 50 mm/s, respectively (indicated as samples ILC-5 and ILC-50), as shown in Fig. 2(c).

The presence of the three additional laser cuts was chosen to obtain a larger ratio of thermally affected material to base material. Figs. 2(a-c) show a schematic of the samples that were analysed using the DSC technique. In the DSC measurements, the heating/cooling rate was 10 °C/min and the temperature ranged between 0 °C and 100 °C.

Thermo-mechanical testing was also performed on samples that were similar to those used for the DSC measurements (see Figs. 2 d-e) except for the MC sample, which was not prepared because of the difficulty in mechanically machining such a small sample without distortions. Due to the small dimensions of the specimens (2 mm×20 mm), stress/strain measurements were performed with a highly sensitive load cell (TA Instruments Q800). The samples were subjected to a loading/unloading loop up to a maximum value of 15 N. The stress/strain curves, determined at 30 °C and 100 °C, were plotted using the real section of the samples in order to take into account the lack of material due to the sample cuts.

3. RESULTS AND DISCUSSION

3.1. Morphological and chemical analysis of the cutting edges

During laser microcutting, the long nanosecond pulse regime (160 ns pulse width) of the adopted fibre laser produced a large quantity of melted material, confirming that the laser ablation process has been prevalently operating in a fusion regime [26]. The shielding gas pushed the molten material through the open kerf, leaving an almost spatter free top cut edge.

In Fig. 3, SEM pictures of the entrance and exit sides of the laser cut edges are reported here as part of the investigation of the process conditions. As can be seen in Fig. 3(d), the bottom cut edge was almost closed by the presence of drops of melted material when a single laser pass strategy

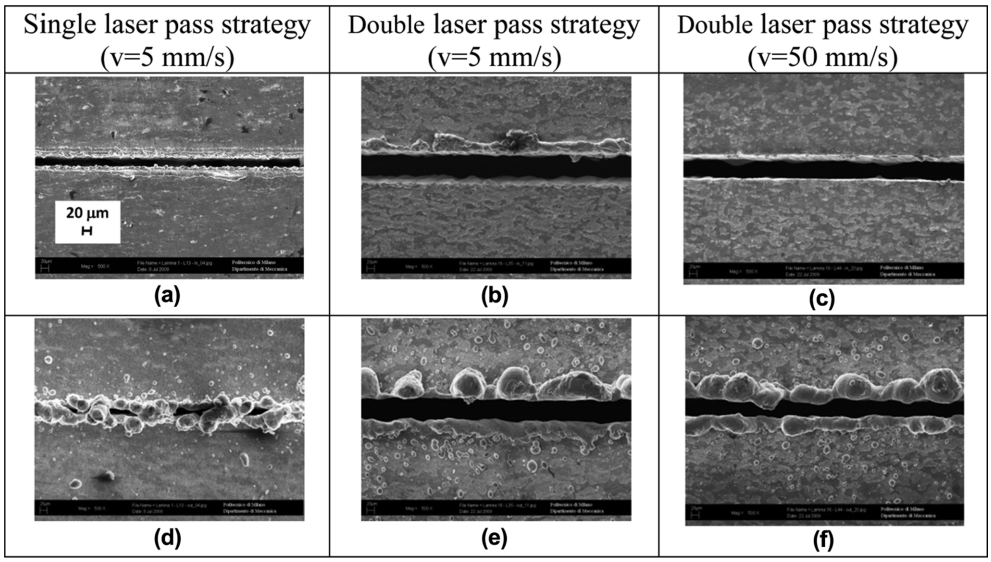

Fig. 3. SEM images of the entrance (a-b-c) and exit (d-e-f) sides of the laser cut edge for a single pass (on the left) and double pass (in the middle and on the right) laser strategy.

with a process speed of 5 mm/s was utilised. The presence of spatter could generate some bridges of melted material between the two sides, and those structures will not allow the generation of a completely open cut edge. This effect is correlated to the very thin kerf width. In fact, bridges of melted material can be generated if the spatter has not been removed from the cut edge by the shielding gas flow.

On the other hand, the double pass cutting strategy allowed a stable through-cut edge to be obtained, as shown in Fig. 3(e-f), even for increased process speeds (i.e., 50 mm/s). When the fixed process speed (i.e., 5 mm/s) with two laser passes is considered, the input energy doubles and consequently the average kerf width was increased from approximately 25 μm in the single pass to 60 μm in the double pass strategy. As the process speed increased from 5 mm/s to 50 mm/s, the top and bottom kerf widths were slightly reduced because of the reduction of the specific energy from 22 J/mm to 2.2 J/mm (see Table 2). Despite the increase of the kerf width, a large quantity of spatter was solidified on the bottom cut edge due to the increased volume of melted material as well as due to the instability of the shielding gas action during the material removal from the bottom kerf. Moreover, the shape of the melted material on the bottom surface looks to be different from the shape created as a function of the process speed [21]. In the double laser pass strategy at low process speed, the spatter was characterised by the presence of some bubbles with irregular distribution along the cutting direction (see Fig. 3e). At the highest process speed, the amount of spatter seemed to not be reduced; instead, its distribution was more regular along the cutting direction (see Fig. 3f). The top surface showed a negligible quantity of spatter at low process speed, while spatter was absent for the highest process speed, as shown in Figs. 3(b-c), respectively.

In Fig. 4, the corresponding transversal and longitudinal sections of the laser cut edges, shown in Fig. 3, are given, in which the presence of spatter on the exit side can be observed. In one particular image, Fig. 4(a), it can be seen that a single laser pass has enough energetic content for a complete melting of the material through the full thickness. This problem causes the closure of the cut edge on the exit side; the problem seems to be due to the generation of spatter and its deposition on the bottom side, as discussed previously. In fact, in Fig. 4(a), it is clear that the laser beam has been able to go through the full thickness of the NiTiCu sheet, but the relevant amount of melted material, shown as something similar to a drop of material under the bottom surface, closes the cut edge. In the case of the second laser pass (double laser pass strategy), shown in Fig. 4(b,c), all the melted material, which solidified inside the cut edge after the first laser pass, was completely removed and a stable cut edge was consequently obtained. As discussed previously, a second effect of the double laser pass strategy has been observed: the enlargement of the kerf, which should make it easier to remove the material during the generation of the laser cut edge.

Finally, in Fig. 4(d), an SEM-SE image of the longitudinal section of a laser cut edge, performed at 22 J/mm, is shown. A layer of melted material on all of the inner surface of the edge, and some irregularities, such as striations [13], were observed, all of which are characteristic of the laser cutting process.

EDS analysis has been performed in order to analyse the chemical composition of the transversal section of the laser cut edge, as shown in Fig. 4(b).

In the table shown in Fig. 4(e), the measured atomic per-

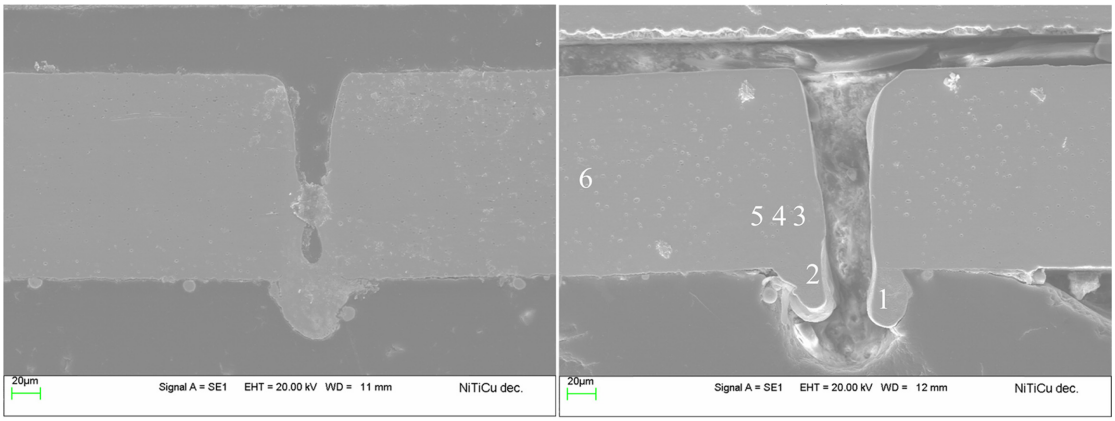

(a) (b)

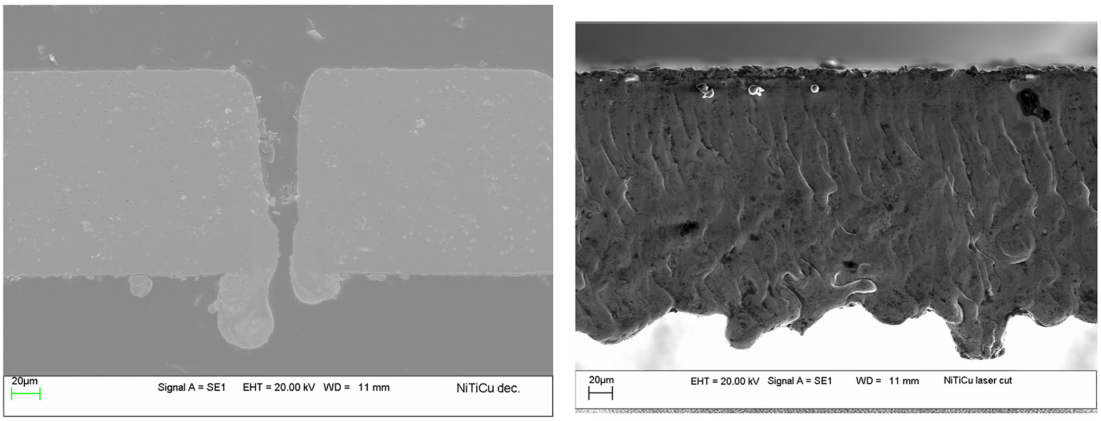

(c) (d)

Spectra	Ti [%at]	Ni [%at]	Cu [%at]
Spectrum 1	49.7	38.8	11.5
Spectrum 2	49.8	38.5	11.7
Spectrum 3	49.1	38.7	12.2
Spectrum 4	49.8	38.3	11.8
Spectrum 5	49.8	38.8	11.5
Spectrum 6	50.4	39.1	10.5

(e)

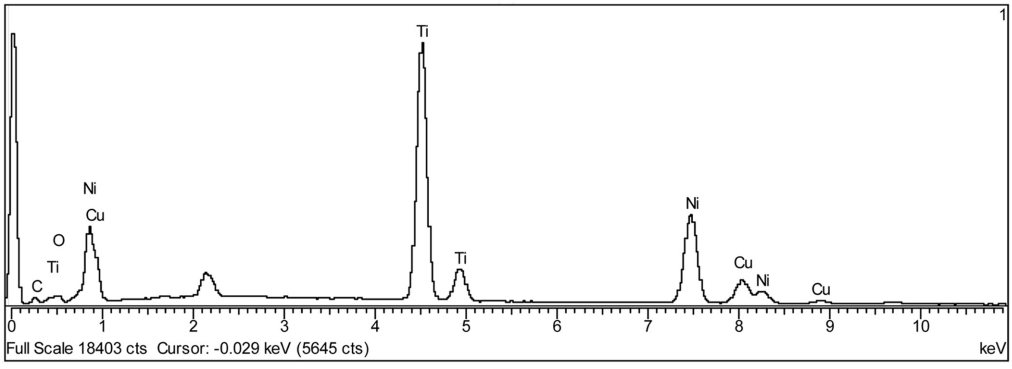

(f)

Fig. 4. SEM images of the transverse sections of the laser cut edge via the single laser pass strategy: single pass - low process speed (a), double pass-low process speed (b), double pass- high process speed (c), longitudinal section of the laser cut edge performed via the double pass - low process speed strategy (d), chemical composition measurements in atomic percentage (e) and a representative spectrum (f), performed on the transverse section of the laser cut edge (see Figure 4(b)).

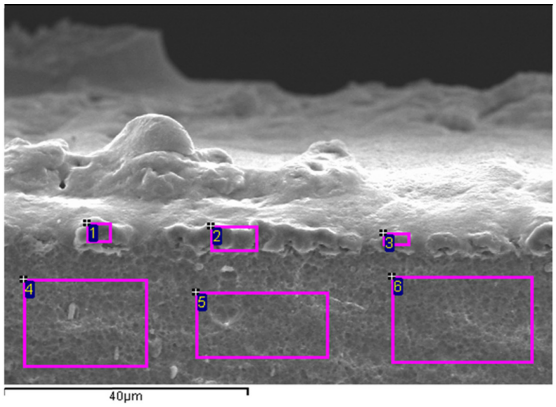

(a)

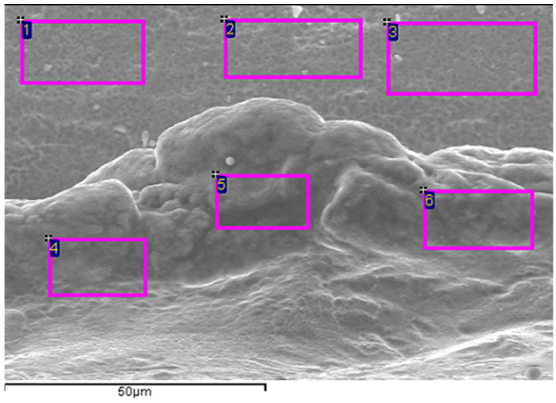

(b)

Spectra	Ti [%at]	Ni [%at]	Cu [%at]
Spectrum 1	74.5	20.3	5.2
Spectrum 2	52.9	36.8	10.3
Spectrum 3	55.4	35.2	9.4
Spectrum 4	50.8	39.1	10.2
Spectrum 5	50.4	39.5	10.2
Spectrum 6	50.0	40.1	9.9

(c)

Spectra	Ti [%at]	Ni [%at]	Cu [%at]
Spectrum 1	51.2	39.2	9.7
Spectrum 2	52.1	38.4	9.4
Spectrum 3	51.5	39.2	9.3
Spectrum 4	60.3	32.7	6.9
Spectrum 5	74.1	21.1	4.8
Spectrum 6	71.3	23.1	5.6

(d)

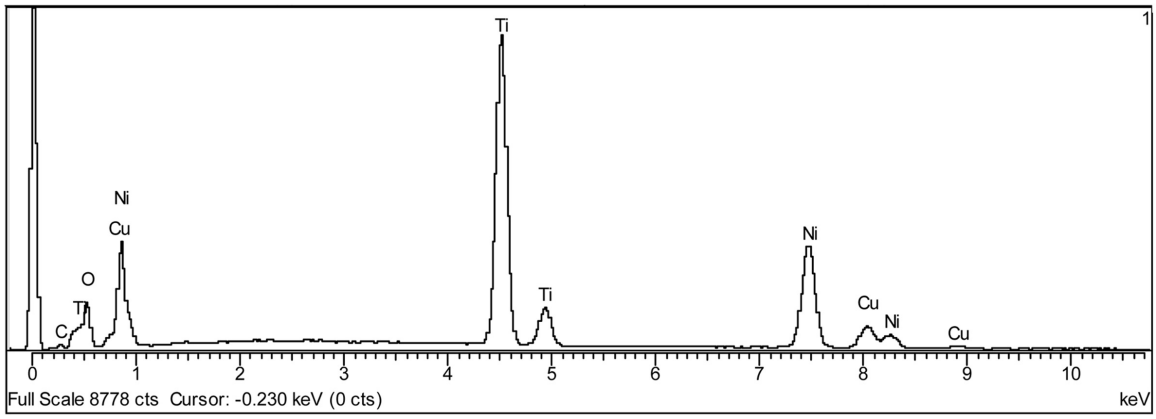

(e)

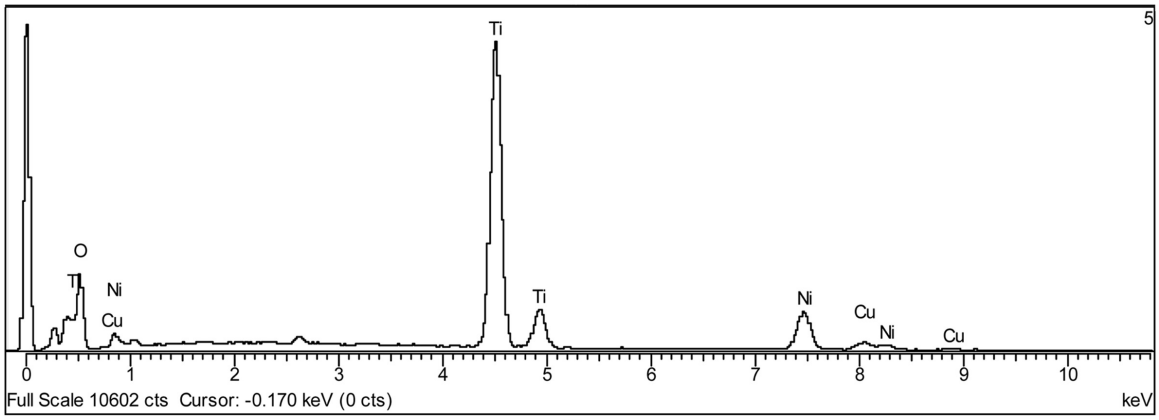

(f)

Fig. 5. Identification of the regions for the chemical composition measurements on the top and bottom surfaces of the laser cut edge (a-b), performed at low process speed with the double laser pass strategy, the chemical composition measurements in atomic percentage (c-d), EDS spectrum of point 1 (e) and 5 (f) on the bottom surface.

centages of the elements of the investigated material (Ni, Ti and Cu) are reported. No significant differences in terms of the chemical composition were found at the analysed points. Moreover, an EDS spectrum, obtained at point 1, showing only the peaks of metallic elements of the SMA, is shown in Fig. 4(f).

SEM and EDS analyses were also performed at the top and bottom surfaces of the laser cut edge for the same process conditions. In Figs. 5(a-b), the magnification of the regions, corresponding to the top and bottom surfaces of the laser cut edge, and the correlated EDS measurements, are respectively reported. Considering the entrance side, as shown in Fig. 5(a), no evident modification of the chemical composition of the sheet, except at point 1, can be observed. This is certainly due to the protecting flow action of the argon. The analysis of the bottom surface shows a sensible variation of the chemical composition with respect to the base material. In fact, in the spatter, the Cu content was significantly reduced and the Ti content was increased, suggesting the generation of surface oxides, such as $Ti_4Ni_2O_x$, for area 4, showing an atomic Ti/Ni ratio of 2:1. In fact, it can be observed that the oxygen signal of the EDS curves is much larger on the exit side due to the spatter when compared to the oxygen signal from the base material.

Moreover, on the external surface a larger amount of Ti has been detected. This could mean that a more stable compound is going to be generated, such as TiO2. This is due to the very fast laser process: the melted material resolidifies before Ti can generate TiO2 on the surface. In fact, TiO2 is not found in any of the samples investigated.

3.2 Nano-indentation analysis of the laser cut edge:

The effect of the laser microcutting was also investigated by evaluating the extent of a HAZ, by means of a determination of the variation of the hardness of the material.

For this purpose, nanoindentation analyses were performed on specimens subjected to two process conditions with completely open bottom kerfs. The positive aspect of this technique is its ability to obtain a high resolution in the spatial domain in order to observe any variation of the mechanical properties from the internal wall of the laser cut edge to the base material. As has previously been shown [27], the use of a nanoindentation test is applicable for the evaluation of the thermal damage induced by the same source during laser microdrilling of commercially pure titanium. This mechanical test can be efficiently adopted to evaluate the HAZ on the order of a few tenths of a micron.

Figure 8 reports the values of the measured nanohardness in the three different regions (top, centre, and bottom) corresponding to the border of the laser cut edges; this measurement was performed at low and high process speeds via the double laser pass strategy. These two process conditions are associated with different specific energy values: 20 J/mm and 2 J/mm, respectively. A clear decrease of the nanohardness values from the cut edge border to the base material was detected. This trend can be observed for both process speed levels as well as for the three considered regions of measurement. The large nanohardness values (450-700 HV) observed in the closest region to the border of the laser cut edge can be associated with a refined microstructure and eventually to material oxidation.

In the case of the low process speed, as shown in Fig. 6(a), the nanohardness values corresponding to the base material were determined to be 40 μm at the border of the laser cut edge, except for the bottom region, where a 20 μm distance was enough to find the base material. As it can be seen in Fig. 6(b), for the high process speed, the base material can be found at a smaller distance (30 μm) from the border of the cut edge in the top and central regions, while the

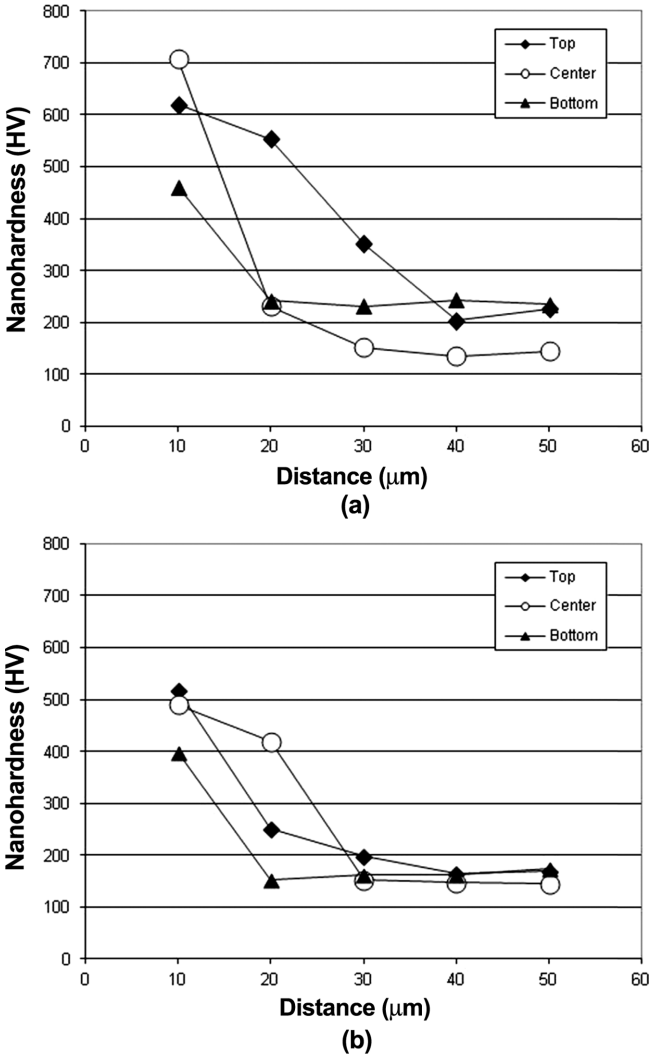

Fig. 6. Nanohardness measurements in the two investigated process conditions: low (a) and high (b) process speed with the double laser pass strategy.

Table 3. Characteristic temperatures and enthalpies of the MT on the different samples

Sample type	H_{heat} [J/g]	A_s [°C]	A_f [°C]	H_{cool} [J/g]	M_s [°C]	M_f [°C]
Sample MC	16.3	47.5	72.2	15.1	61.9	33.5
Sample PLC	13.1	48.6	74.1	15.0	64.1	33.1
Sample ILC-5	11.4	53.7	72.7	13.5	65.2	42.0
Sample ILC-50	14.4	51.5	72.1	14.3	62.3	37.0

base material can be found at the same distance (20 μm) for the bottom region, because of the minor density of energy adopted during the laser microcutting. This means that the extent of the HAZ can be estimated to be in the range of a few tenths of a micron; moreover, the effect of the process speed can be evidently associated with the different sizes of the HAZ.

3.3. Calorimetric and thermo-mechanical analysis of the material

The presence of thermal alterations was confirmed by calorimetric analysis, as shown in Fig. 9, which shows the DSC scans of the samples depicted in Fig. 2. Martensitic transformation (MT), occurring due to the processing conditions, can be revealed by the presence of heat flow peaks. The base material (sample MC) presents a single peak, typical of cold worked and low temperature (400 °C) thermally treated materials. For the laser cut specimens, the DSC curves are characterised by multiple overlapping peaks, reflecting the presence of different microstructures described as the base material, the thermally affected zone, and melted material. The base material is characterised by a lower hardness (see Fig. 8) and a DSC scan with features typical of a slightly cold worked NiTiCu alloy.

Due to the heat introduced during the laser process, the shape of the MT peaks is more complex and a multiple step transformation is detected. That transformation is related to the different microstructures in the HAZ/melted zones.

In Table 3, the characteristic temperatures and the corresponding MT enthalpies of the DSC scans shown in Fig. 7 are presented. The results show that the MT temperatures increased and the corresponding enthalpies slightly decreased in average from approximately 15 J/g to 12 J/g with the increase of the amount of heat during the laser cutting process.

Moreover, the mechanical test results shown in Fig. 8 confirm that, even in a less evident way, the laser machining introduces an effect on the SMA from a mechanical point of view. At both test temperatures of 30 °C and 100 °C, which respectively correspond to the full martensitic and the full austenitic conditions, the behaviours of the three analysed

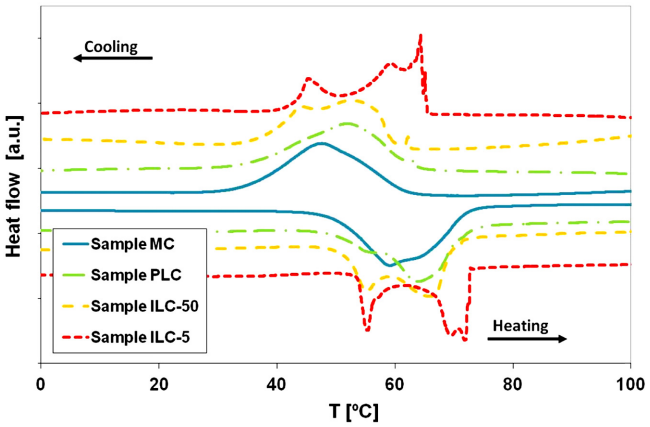

Fig. 7. DSC scan of the different samples used to investigate the effect of laser microcutting process.

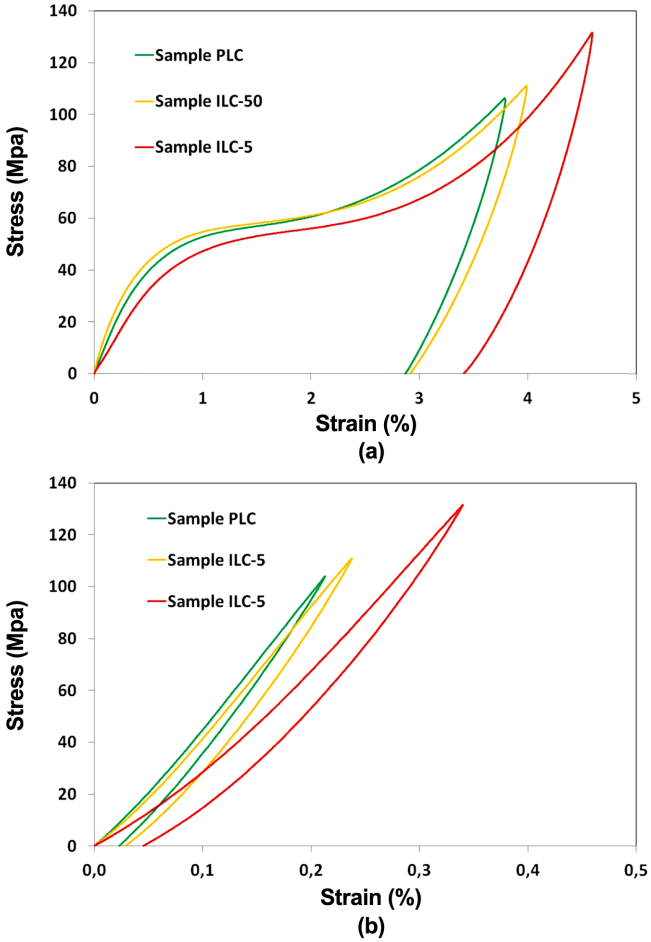

Fig. 8. Stress-strain curve, obtained in tensile configuration, for the laser cut samples in martensite (a) and austenite (b) phase.

samples are different. A reduction in the plateau stress value at the low temperature and a decrease of the apparent elastic modulus at the high temperature are observed. Both values are known to be related to the residual cold work inside the sample [28]: the more annealed the material is, the lower the values become. This softening can be clearly observed for Sample ILC-5; on the contrary, Sample ILC-50 looks very similar to Sample PLC. This evidence confirms that in the case of Sample ILC-50, which has an overall behaviour quite similar to that of Sample PLC, the thermal alteration not only spans a reduced distance from the cut edge, but its intensity is also reduced. Finally, an increase of the Young's modulus can be observed in Fig. 8 when the low process speed is utilised; consequently, the material rigidity as well as the increased hardness, shown in Fig. 8, can be associated with the heat.

4. CONCLUSIONS

In this work, the effect of the microcutting process, performed with a nanosecond fibre laser on a 150 mm thick NiTiCu SMA sample, on the metallurgical and thermo-mechanical properties was studied. The main conclusions that were drawn are as follows:

(1) An effect of the process speed at two levels (5 mm/s and 50 mm/s) is observed on the geometry and the dimensions of the laser cut edge. The presence of melted material, mainly found on the exit side, can be associated with the pulse width in the nanosecond regime of the laser source used. A fine kerf, on the order of a few tenths of a micron, can be obtained by using a pulsed fibre laser.

(2) The presence of a higher oxygen content measured in the proximity of the laser cut edge is due to the high temperatures reached during the laser cutting process; the added heat creates an area that demonstrates stronger oxidation. This effect can be associated with a relevant thermal cycle, imposed by the laser beam, which means that there is a thermal damage effect on the properties of the SMA.

(3) An evaluation of the dimensions of the HAZ is performed via nanohardness measurements in proximity of the laser cut edge on the transversal section. The effect of the investigated process speed is significant on the extent of the HAZ; the HAZ can be estimated to be located from 30 mm to 40, corresponding to processing speeds of 50 mm/s and 5 mm/s, respectively.

(4) Calorimetric analysis using the DSC technique was performed on the laser cut samples with different configurations. This analysis showed how the heat introduced by the laser machining has a clear effect in terms of modification of the shape of the MT peaks.

(5) Thermo-mechanical characterisation was used to confirm a consistent thermal alteration for the sample processed at low speed whilst the sample processed at high speed behaved similarly to the non-processed material. An increase of the elastic modulus was observed when a larger amount of heat was introduced into the material during the laser machining.

It can be concluded that the thermal alterations were confirmed by the results seen on the NiTiCu SMA cut with a nanosecond fibre laser and that the presence of thermal alterations has to be taken into account when this material is used in industrial applications that require particular calorimetric properties.

REFERENCES

1. K. Otsuka and C. M. Wayman, *Shape Memory Materials,* Cambridge Univesity Press (1998).
2. T. Duerig, A. Pelton, and D. Stockel, *Mater. Sci. Eng. A* **273-275**, 149 (1999).
3. N. Muhammad, D. Whitehead, A. Boor, W. Oppenlander, Z. Liu, and L. Li, *Appl. Phys. A*, **6609-4**, 607 (2010).
4. M. Kohl, B. Krevet, and E. Just, *Sensors Actuat. A* **97-98**, 646 (2002).
5. M. Leester-Schadel, B. Hoxhold, C. Lesche, S. Demming, and S. Buttgenbach, *Microsyst. Technol.* **14**, 697 (2008).
6. M. Rohde and A. Schussler, *Sensors Actuat. A* **61**, 463 (1997).
7. A. Schuessler, *Proc. of SMST* (eds. S. Russell and A. Pelton Asilomar), pp.25-32, Pacific Grove, California, USA (2000).
8. J. Meijer K. Du, A. Gilner, D. Hoffmann, V. S. Kovalenko, T. Masuzawa, A. Ostendorf, R. Poprawe, and W. Schulz, *CIRP Annals–Man Tech.* **51**, 531 (2002).
9. J. Meijer, *Journal of Mater. Proc. Tech.* **149**, 2 (2004).
10. M. Trtica, *Appl. Surf. Sci.* **253**, 2551 (2006).
11. K. C. Yung, H. H. Zhu, and T. M. Yue, *Smart. Mater. Struct.* **14**, 337 (2005).
12. C. Li, S. Nikumb, and F. Wong, *Opt. Laser Eng.* **44**, 1078 (2006).
13. B. Tirumala Rao, R. Kaul, P. Tiwari, and A. K. Nath, *Opt. Laser Eng.* **43**, 1330-1348 (2005).
14. I. A. Almeida, W. De Rossi, M. S. F. Lima, J. R. Berretta, G. E. C. Nogueira, N. U. Wetter, and N. D. Viera Jr., *Journal of Mat. Proc. Tech.* **179**, 105 (2006).
15. R. Pfeifer, D. Herzog, M. Hustedt, and S. Barcikowski, *Journal of Mat. Proc. Tech.* **210**, 1918 (2010).
16. M. Baumeister, K. Dickmann, and A. P. Hoult, *Appl. Phys. A* **85**, 121 (2005).
17. H. Meng, J. Liao, Y. Zhou, and Q. Zhang, *Opt. Laser Technol.* **41**, 300 (2009).
18. A. G. Demir, B. Previtali, D. Colombo, Q. Ge, M. Vedani, L. Petrini, W. Wu, and C. A. Biffi, *Proc. SPIE 8237* (eds Eric C. Honea), 8237730/1-9, California, USA (2012).
19. A. Ancona, F. Röser, K. Rademaker, J. Limpert, S. Nolte, and A. Tünnermann, *Opt. Express* **16**, 8958 (2008).
20. L. Shah, M. E. Fermann, J. W. Dawson, and C. P. J. Barty , *Opt. Express* **14**, 12 (2006).
21. B. Previtali, S. Arnaboldi, P. Bassani, C. A. Biffi, N. Lecis, A. Tuissi, M. Carnevale, and A. LoConte, *Proc. of ESDA*,

pp. 593-602, ASME, Istanbul, Turkey (2010).
22. P. Bassani, C. A. Biffi, M. Carnevale, N. Lecis, B. Previtali, and A. LoConte, *Mater. Design* **45**, 88 (2013).
23. C. A. Biffi, P. Bassani, A. Tuissi, M. Carnevale, N. Lecis, A. LoConte, and B. Previtali, *Funct. Mate. Let.* **5**, 1 (2012).
24. A. Tuissi, S. Besseghini, T. Ranucci, F. Squatrito, M. Pozzi, *Mater. Sci. Eng. A* **273-275**, 813 (1999).
25. A. Nespoli, C. A. Biffi, R. Casati, E. Villa, A. Tuissi, and F. Passaretti, *New Developments on Mini/Micro Shape Memory Actuators, Smart Actuation and Sensing Systems - Recent Advances and Future Challenges* (ed. Giovanni Berselli, Rocco Vertechy and Gabriele Vassura,), pp.35-52, Intech, Croatia (2012).
26. S. S. Kudesia, P. Solana, W. Rodden, D. P. Hand, and J. Jones, *J. Laser. Appl.* **14**, 3 (2005).
27. C. A. Biffi, N. Lecis, B. Previtali, M. Vedani, and G. Vimercati, *Int. J. Adv. Manuf. Tech.* **51**, 9 (2010).
28. C. Grossmann, J. Frenzel, V. Sampath, T. Depka, A. Oppenkowski, and Ch. Somsen, *Mat.-wiss. u. Werkstofftech* **39**, 8 (2008).